MODELING OF PROPELLER-WING AERODYNAMICS FOR AIRCRAFT FEATURING LARGE NUMBER OF CONTROL DEVICES

H.-J. Steiner, M. Hornung
Bauhaus Luftfahrt
Lyonel-Feininger-Str. 28, 80807 München, Deutschland
S. Baur, F. Holzapfel
Technische Universität München, Lehrstuhl für Flugsystemdynamik
Boltzmannstr. 15, 85748 Garching, Deutschland

Abstract

A framework of methods for calculating aerodynamic forces and moments of aircraft configurations with strong propeller-wing coupling is presented and applied for a UAV with a large number of control inputs. A nonlinear lifting-line method is used for the calculation of lifting surface aerodynamics. By the use of nonlinear two-dimensional airfoil data the method yields good results even at angles of attack beyond stall. Blade element theory combined with momentum theory and Goldstein's assumption is used to calculate the propeller forces and moments as well as the induced flow field in the propeller slipstream. Lifting surface and propeller aerodynamics are coupled in an iterative way to model the mutual influence on each other. The induced velocity of bodies of revolution is modeled based on slender body theory and superimposed on the free stream to yield the influence on lifting surfaces and propellers.
The methods are used to calculate the aerodynamic dataset for a simulation model of a UAV with strong propeller-wing coupling and a large number of control inputs. An approach is presented for identifying the interdependence of flight states and control inputs to allow for an optimized design of computational experiments. The goal of this optimization process is to generate an aerodynamic dataset containing as much information about the system as possible with a given limited number of computations.

1. NOMENCLATURE

a	Speed of sound
ρ	Density
ν	Kinematic viscosity
C_l, C_d, C_m	Airfoil lift, drag and moment coefficient
C_D, C_Q, C_L	Drag, cross-flow and lift coefficient
C_l, C_m, C_n	Rolling moment, pitching moment and yawing moment coefficient
L, D, M	Lift force, drag force, pitching moment
p, q, r	Roll rate, pitch rate, yaw rate
p^*, q^*, r^*	Dimensionless roll-, pitch- and yaw rate
$C_{l\alpha}$	Airfoil lift curve slope
α_{l0}	Airfoil zero lift angle of attack
T	Thrust force
A	Propeller disk area
$\Delta_z y$	Additive effect on output variable y due to input variable z

Symbols not listed here are explained within the text.

2. INTRODUCTION

Knowledge of the aerodynamic characteristics of aircraft configurations is a key element for aerospace disciplines like preliminary aircraft design, control and stability analysis or flight control system development. Especially for configurations with strong propeller-wing coupling the influence of the propeller(s) on the aircraft aerodynamics is an aspect that has to be considered already during the preliminary aircraft design and for control and stability evaluations (e.g. for configurations with propeller powered high-lift or with distributed thrust). These tasks demand a fast responding tool for calculating aerodynamic forces and moments of arbitrary wing-propeller configurations (allowing for modeling of conventional as well as unconventional aircraft configurations like e.g. Box Wing, Tilt Wing, etc.), including also good approximations of nonlinear aerodynamic characteristics at angles of attack beyond stall.

Numerous methods have been developed in the field of propeller-wing aerodynamics, ranging from handbook methods (e.g. the USAF DATCOM [1]) over potential flow methods up to computational fluid dynamics. In the field of conceptual aircraft design, blade element methods and helical vortex models used to model the flow field of the propeller have been coupled to panel methods, vortex lattice methods or lifting-line methods in order to predict the aerodynamic characteristics of propeller-wing combinations [2],[3],[4].
For the purpose of preliminary aircraft design, Stone presented a method combining a full azimuthal blade-element solution, modeling the propeller aerodynamics, with a panel method [5]. The panel method results were corrected using two-dimensional viscous airfoil data to account for viscous effects e.g. at angles of attack beyond stall. Yet, because of computational reasons, there has been no attempt to iterate the viscous solution. Also only the impact of the propeller slipstream on the wing has been considered and there was no iteration of the propeller solution and the wing solution.
Another approach for modeling the propeller-wing interaction was conducted by Hunsaker and Snyder [6].

They used a blade element propeller solution coupled to a lifting-line method [7]. The method allows for modeling of nonlinear effects by iteratively solving the lifting-line equations using 2-D airfoil data.

The goal of this work is to combine aerodynamic methods partly based on the work of Hunsaker and Snyder with a tool framework for generic and flexible geometry generation and modification. The resulting framework shall allow for the calculation of aircraft aerodynamics with propeller-wing interaction for preliminary design purposes. It shall be capable of the generation of aerodynamic datasets for aircraft design, control and stability analysis and flight simulation, thereby offering the possibility to handle a broad spectrum of control device inputs. Based on the lifting-line method described by Phillips and Snyder, a tool has been implemented that offers a flexible platform for generating and analyzing aircraft geometries with arbitrary number of lifting surfaces, propellers and bodies of revolution featuring also complex kinematic dependencies.

As an example application an aerodynamic dataset for a UAV with strong propeller-wing coupling and a large number of control devices is generated. The dataset shall be used for a dynamic simulation model of the UAV. Due to the large number of independent variables (flight states and control inputs) required for the generation of the aerodynamic dataset, a full-factorial design space exploration results in high computational effort. A methodical approach is presented for identifying the interdependence of control inputs. This allows for an optimal selection of the points in the multidimensional control space to be computed, in order to achieve an optimal representation of the system behavior for a given limited computational time.

3. HIERARCHICAL GEOMETRY PARAMETERIZATION

An object orientated treatment of the geometry has been implemented to generate a hierarchy based geometry model. The geometry is created by setting up a tree structure of frame objects by using collection objects, that are able to contain further frame objects (see FIG 1).

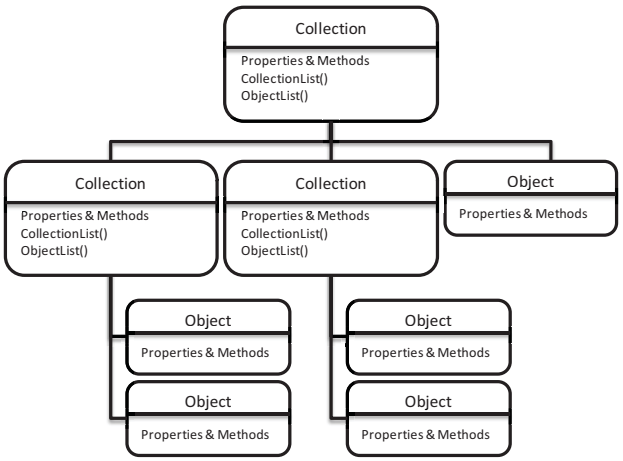

FIG 1. Sketch of the hierarchical tree structure used for geometry representation

Each frame object possesses an object COS (coordinate system) (O) and has the following properties that relate the object to its parent object (P) in the tree structure:

- Position of object COS origin relative to parent COS, components given in parent COS: $\left(\vec{r}^{\,PO}\right)_P$
- Velocity of object COS origin relative to parent COS with respect to parent COS, components given in parent COS: $\left(\vec{V}^{\,PO}\right)_P^P$
- Orientation of object COS relative to parent COS given by a transformation matrix M_{PO}
- Angular rate of object COS relative to parent COS, components given in parent COS: $\left(\vec{\omega}^{\,PO}\right)_P$

This information is used to calculate the position and velocity of an arbitrary point C (e.g. a panel reference point given in the local object COS) relative to the parent object frame (see FIG 2):

(1) $$\left(\vec{r}^{\,PC}\right)_P = \left(\vec{r}^{\,PO}\right)_P + M_{PO} \cdot \left(\vec{r}^{\,OC}\right)_O$$

(2) $$\left(\vec{V}^{\,PC}\right)_P^P = \left(\vec{V}^{\,PO}\right)_P^P + M_{PO} \cdot \left(\vec{V}^{\,OC}\right)_O^O + \left(\vec{\omega}^{\,PO}\right)_P \times M_{PO} \cdot \left(\vec{r}^{\,OC}\right)_O$$

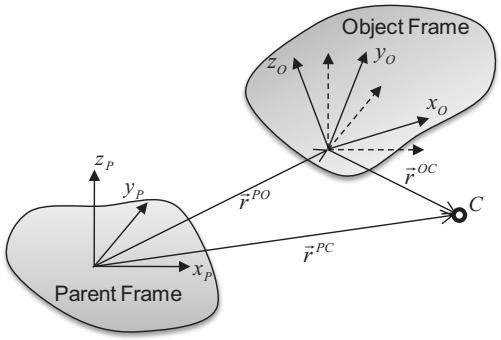

FIG 2. Relation between parent frame coordinate system and object frame coordinate system

This transformation chain is continued from every object up to the tree top node, which represents the reference frame of the aircraft configuration. This way the geometric and kinematic properties of every object are transformed to the reference COS.

Different types of frame objects are used to create an aircraft geometry:

- Collections serve as frames that can comprehend lists of frame objects (including further collections). They allow to perform actions on all sub-objects[1].
- Lifting Surface frame objects represent a lifting surface with the appropriate properties and methods.
- Rotor frame objects represent a rotor/propeller with the appropriate properties and methods.
- Body frame objects represent a body of revolution with the appropriate properties and methods.

By implementing a recursive search algorithm, arbitrary tree structures consisting of the described frame objects can be created and treated without explicit knowledge of the current tree structure or need of adapting the code.

With the presented hierarchical tree structure the geometry of arbitrary aircraft configurations consisting of a number of components (e.g. lifting surfaces, propellers or bodies of revolution) can be easily modeled, including complex kinematic relations.

[1] Actions performed on a tree structure are for example the generation of computation meshes, the calculation of total forces and moments or the plotting of all objects contained in a geometry structure.

4. MODELING OF PROPELLER-WING AERODYNAMICS

The basic modeling aspects used by the implemented methods are described in the following. The aerodynamic methods applied are based on momentum theory (for modeling the induced velocity of propellers) and potential flow theory (application of singularities like vortices and concept of superposition). All geometries (except bodies of revolution) can be described as lifting surfaces with the following modeling concepts arising from this approach:

- The geometry is modeled using spanwise discretization of the lifting surfaces into wing segments.
- Two-dimensional airfoil data is used to model the aerodynamic characteristics of these wing segments.
- The aerodynamic influence of objects on each other and on the object itself is modeled using the concept of induced velocities.

The limitations arising from this modeling approach are:

- Geometry is constrained to lifting surfaces with a reasonable high aspect ratio (≥ 4) to legitimate the two-dimensional flow modeling.
- Modeling of viscosity and compressibility effects is limited to the information contained in the 2-D airfoil data.
- No modeling of three-dimensional flow effects due to spanwise pressure gradients is considered (only three-dimensional flow described by vortex theory is modeled).

A wing segment or panel is described by the position of its reference point R and by its orientation, given by the panel coordinate system (see FIG 3). The position of the panel reference point is located on the wing quarter chord line. The aerodynamic force and moment acting on the panel is calculated from the local flow velocity evaluated at the panel reference point, which is used to calculate the panel angle of attack α, the panel Reynolds number Re, the panel Mach number Ma and the panel dynamic pressure $\bar{q}$. Based on this aerodynamic panel data and the panel flap deflection δ, the aerodynamic airfoil coefficients are evaluated using either analytical models or interpolation of airfoil data stored in multidimensional data tables. The panel aerodynamic force and moment is then calculated with the panel area S and the panel chord length c_R.

$$(3)\quad \left(\vec{F}\right)_{Pan} = \begin{bmatrix} \cos\alpha & 0 & -\sin\alpha \\ 0 & 1 & 0 \\ \sin\alpha & 0 & \cos\alpha \end{bmatrix} \begin{pmatrix} C_d(\alpha, Re, Ma, \delta) \\ 0 \\ C_l(\alpha, Re, Ma, \delta) \end{pmatrix} \cdot \bar{q} S$$

$$(4)\quad \left(\vec{M}\right)_{Pan} = \begin{pmatrix} 0 \\ C_m(\alpha, Re, Ma, \delta) \\ 0 \end{pmatrix} \cdot \bar{q} S c_R$$

with

$$(5)\quad Re = \frac{V \cdot c_R}{\nu} \qquad Ma = \frac{V}{a} \qquad \bar{q} = \frac{\rho}{2} \cdot V^2$$

$$(6)\quad \alpha = \tan^{-1}\left(\frac{\begin{bmatrix} 0 & 0 & 1 \end{bmatrix} \cdot \left(\vec{V}_F^R\right)_{Pan}}{\begin{bmatrix} 1 & 0 & 0 \end{bmatrix} \cdot \left(\vec{V}_F^R\right)_{Pan}} \right)$$

and the magnitude of the flow velocity projected on the panel x-z-plane being (see FIG 3)

$$(7)\quad V = \left\| \begin{bmatrix} 1 & 0 & 0 \\ 0 & 0 & 0 \\ 0 & 0 & 1 \end{bmatrix} \cdot \left(\vec{V}_F^R\right)_{Pan} \right\|$$

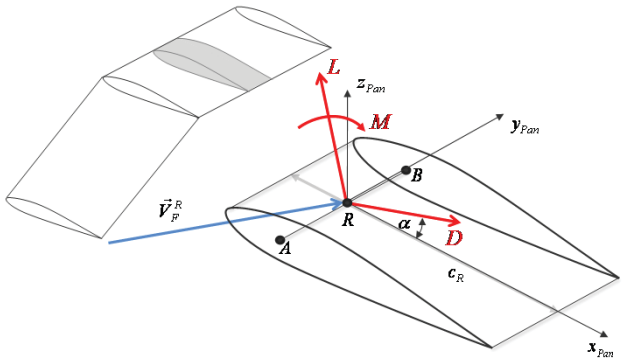

FIG 3. Definition of panel properties

The local flow velocity is composed of the aerodynamic linear and angular velocity of the aircraft w.r.t. the atmosphere, the relative kinematic velocity of the panel reference point w.r.t. the aircraft reference frame (e.g. due to component rotation or tilting) and the aerodynamic induced velocity due to other components, evaluated at the panel reference point.

4.1. Propeller and Slipstream Model

4.1.1. Propeller Model

The implemented propeller model is based on a blade element approach, i.e. the propeller blades are radially divided into blade elements. Additionally the propeller is modeled by a number of azimuthal blade positions to account for non-axial flow conditions and periodical geometry changes like blade flapping and blade pitching. For every blade element the local flow velocity consisting of the aerodynamic and kinematic velocity and the induced velocity is calculated. Based on this velocity the aerodynamic force and moment of the blade element is calculated according to equations (3) and (4) using two-dimensional airfoil data. The resulting steady propeller force and moment is calculated by summing all element forces and moments divided by the number of azimuthal positions and multiplied by the number of blades.

Different models have been implemented to calculate the self-induced velocity at the propeller blades. For each propeller component of the aircraft geometry one of the following methods can be chosen:

- Simple momentum theory [8] (no radial variation of self-induced velocity).
- Blade element momentum theory [9] (using circular annuli for calculation of self-induced axial velocity) with optional calculation of the tangential velocity based on Goldstein's assumption [10].
- Goldstein theory [11] (using vortex theory for calculation of the induced axial and tangential velocity).

The principle of momentum theory is to calculate the induced velocity from the thrust acting on the propeller. In simple momentum theory the rotor is treated as one continuous blade disk with one induced axial velocity normal to the blade disk and one average external flow velocity acting on the propeller disk. A modification for external velocities not parallel to the propeller axis according to McCormick [12] is applied to solve for the axial induced velocity in an iterative way.

For the blade element momentum theory the momentum principle is applied to annular rings of the propeller to get a radial distribution of the induced axial velocity based on the radial distribution of thrust. The induced tangential velocity is calculated from the induced axial velocity by applying Goldstein's assumption, stating that the total induced velocity at a blade element reference point is perpendicular to the resulting total flow velocity at the blade element reference point. This condition leads to a quadratic equation for the tangential induced velocity.

Alternatively a Goldstein vortex theory according to [11] has been implemented to solve for the induced axial and tangential velocity at the propeller disk. To apply the theory for non axis-symmetric cases all values are taken as averaged mean values over all azimuthal stations.

4.1.2. Slipstream Model

In order to model the interaction of the propeller aerodynamics with other components like wings or propellers, the induced velocity within the propeller wake has to be modeled. This is done based on the induced axial and tangential velocities in the propeller plane, which were calculated in the appropriate propeller induced velocity model. Mass conservation and vortex theory is applied to model the induced velocity in the rotor wake. From vortex theory a wake contraction factor k_d is calculated according to McCormick [12],

$$(8)\quad k_d = 1 + \frac{s}{\sqrt{s^2 + R^2}}$$

which is used as a factor ranging from 1 to 2 to calculate the development of the axial induced velocity at an axial distance s from the propeller plane with radius R.

The radius of the rotor wake R_{Wake} at an axial distance s from the rotor plane is calculated from mass conservation according to [5]

$$(9)\quad R_{Wake} = \sqrt{r_N^2 + \sum_{k=1}^{n_k} \left(r_{A,k+1}^2 - r_{A,k}^2\right) \cdot \frac{V_{a,k}^{ext} + w_{ind,k}}{V_{a,k}^{ext} + k_d \cdot w_{ind,k}}}$$

where r_N is the nacelle radius modeled as a function of s, $r_{A,k}$ is the inner radius of the k-th propeller discretization annulus, $V_{a,k}^{ext}$ is the axial component of the external flow velocity at the k-th annulus and $w_{ind,k}$ is the induced axial velocity at the propeller plane at the k-th annulus.

The induced velocity distribution at the propeller plane (induced axial and tangential velocity) is mapped onto the wake plane at axial distance s using linear interpolation and a reduction of the induced velocity to zero at the slipstream boundary. The axial induced velocity in the propeller wake is calculated by multiplying the interpolated value with the factor k_d. The tangential induced velocity in the propeller wake is determined by a velocity jump to twice the propeller plane value immediately behind the disc and an afterwards increase in order to preserve angular momentum.

4.2. Aerodynamic Model

4.2.1. Lifting Surfaces

The lifting-line method used for calculation of wing aerodynamics is based on the method described by Phillips and Snyder [6] and constitutes an adaptation of the classical lifting-line theory, applying a three-dimensional vortex lifting law instead of the two-dimensional Kutta-Joukowski law used in classical theory. This enables the method to be used for systems of lifting surfaces with arbitrary camber, sweep and dihedral. Further the method is able to account for nonlinear airfoil data by solving a nonlinear equation system.

The aerodynamics of a lifting surface is synthesized using a composite of horseshoe shaped vortices, which model the distribution of bound vorticity over the surface of the wing and the distribution of free vorticity in the trailing vortex sheet in a discrete way. The bound portion of each horseshoe vortex is placed coincident with the wing quarter chord line. The trailing vortices are aligned either to the free stream velocity or to the local flow velocity. The trailing vortices may be modeled to follow the wing surface (including a flap deflection) and leave the wing at the trailing edge.
The *Biot-Savart* law can be applied to determine the resulting induced velocity at any point in space, if the circulation strength Γ of each horseshoe vortex is known. However, these strengths are not known a priori, but are the unknown variables to be calculated. To compute the vortex strengths of the n vortices, a system of n equations has to be solved. These equations can be found by relating the circulation strength of a panel i to the aerodynamic force vector acting on that panel

$$(10)\quad \vec{F}_i = \rho \cdot \Gamma_i \cdot \vec{V}_F^{R_i} \times \left(\vec{r}^{\,OB_i} - \vec{r}^{\,OA_i}\right)$$

and the magnitude of the aerodynamic force vector to the aerodynamic and geometric properties of the panel

$$(11)\quad \left|\vec{F}_i\right| = \frac{\rho}{2} \cdot V_i^2 \cdot C_{l,i}\left(\alpha_i, Re_i, Ma_i, \delta_i\right) \cdot S_i$$

where V_i is the magnitude of the flow velocity at the panel reference point projected into the panel x-z-plane.

Combining equation (10) and (11) results in a n-th order nonlinear equation system, because the flow velocity (and dependent on that the angle of attack, the Reynolds number and the Mach number) is a function of the n circulation strengths. This equation system can either be solved using nonlinear equation solving techniques like e.g. a Jacobian based Newton method. Alternatively the equation system can be linearized applying small angle of attack approximations and linearization of the airfoil data:

$$(12)\quad C_{l,i}\left(\alpha_i, Re_i, Ma_i, \delta_i\right) \cong C_{l\alpha,i} \cdot \left(\alpha_i - \alpha_{l0,i} + \varepsilon_{f,i} \cdot \delta_i\right)$$

with the flap effectiveness $\varepsilon_{f,i} = \sqrt{c_{f,i}}$ as a function of the relative flap chord length $c_{f,i}$ according to [13].

Although the linearization is only valid for angles of attack within the linear airfoil range, it has been found that good approximation of aerodynamic characteristics beyond stall

is also achieved when using the linearized equation system to calculate the induced velocities. This is due to the fact, that nonlinear airfoil data is used for calculating the aerodynamic forces and moments based on the induced velocities. In this case the calculation of the induced velocities normally overestimates the induced effects due to the use of linear airfoil data. The use of nonlinear airfoil data however to calculate the aerodynamic forces and moments allows for nonlinear effects to be considered partly.

4.2.2. Bodies of Revolution

A hybrid approach is used for modeling aerodynamics of bodies of revolution. The induced velocity field of a body is modeled using slender body theory. The flow past a body of revolution is decomposed into an axial displacement flow and a cross flow perpendicular to the body axis [14]. The axial flow is modeled using a discrete point source distribution on the body axis. The cross flow is modeled using a discrete point doublet distribution on the body axis pointing in direction of the cross flow. The strength of the singularities is calculated using the body contour as boundary condition. The body-induced velocity is evaluated at the lifting surface and propeller panel reference points to model the influence of the body displacement flow. The aerodynamic forces and moments of the body are calculated using empirical methods according to DATCOM [1].

4.3. Propeller-Wing Interaction

When calculating configurations composed of wings and propellers, these components are aerodynamically interacting with each other. The induced velocity of propeller components influences the aerodynamics of lifting surfaces inside the propeller slipstream, and the induced velocity field of lifting surfaces is influencing the flow at the propeller blades. The lifting surface and propeller aerodynamics are coupled by calculating the system in an iterative way: The propeller aerodynamics is calculated as described in section 4.1 and the induced velocity in the propeller slipstream is added to the flow velocity at the wing panel reference points. The wing aerodynamics is then calculated based on the resulting total flow velocity and the wing-induced velocity field is superimposed on the flow velocity at the propeller blade element reference points. This process is repeated until the value of the wing-induced velocity at the propeller has converged or a maximum number of iterations is reached. After the final iteration the aerodynamic forces and moments of wings and propellers are calculated based on the resulting induced velocities. The induced velocity concept allows capturing the mutual influence of propeller and wing aerodynamics to some extent with only one calculation of the wing and propeller induced velocities.

4.4. Comparison with Experimental Data

To validate the methods implemented for wing and propeller aerodynamics, two test cases are presented providing experimental data for a single tapered wing and a wing-propeller combination.

4.4.1. Validation of the Lifting-Line Method

To validate the implemented lifting-line method, an unswept, single tapered wing according to the NACA TN-1270 report [15] has been calculated. The main geometric and aerodynamic properties of the chosen case are listed in TABLE 1.

Property	Value
Wing span	10.75 m
Wing aspect ratio	8
Wing taper ratio	0.4
Wing MAC	1.43 m
Wing airfoil (root)	NACA4415
Wing airfoil (tip)	NACA4412
Reynolds number	4.32×10^6
Mach number	0.13

TABLE 1. Geometric and aerodynamic properties of validation test case according to NACA TN-1270 [15].

Based on the experimental data an angle of attack range from -5° to 21° has been calculated. FIG 4 shows the results of the calculation including the result from the public vortex lattice method Tornado (VLM) [16]. The lifting-line method results were calculated using the linear solver, with the non-linear airfoil data based on diagrams from Abbott [17] for NACA4412 and NACA4415 airfoils. A spanwise cosine discretization of 10 panels has been used for both the lifting-line and the VLM tool. The VLM mesh was created using three chordwise panels.

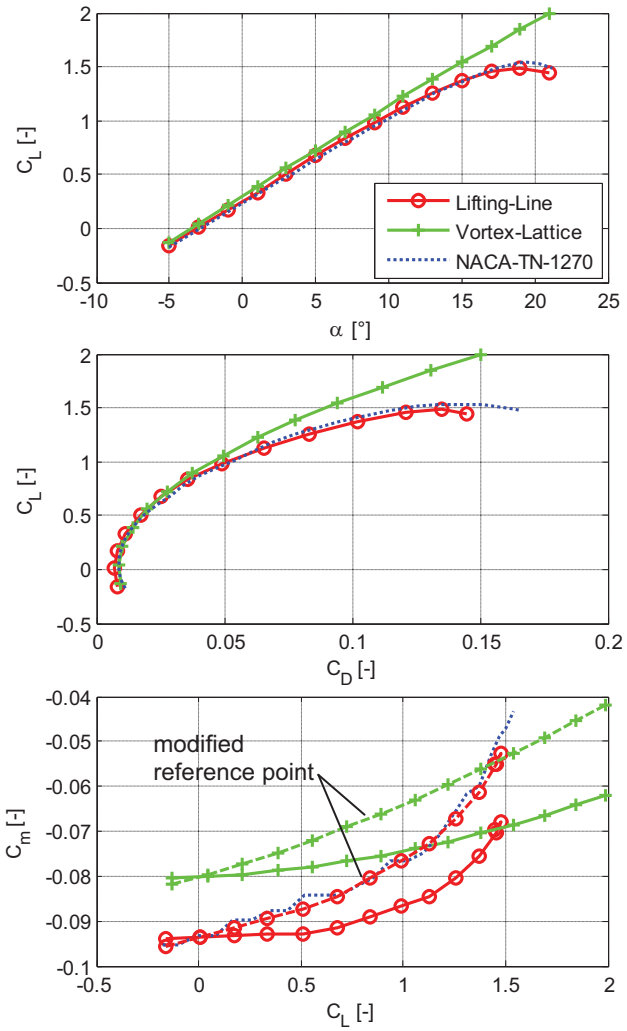

FIG 4. Calculated and experimental results for a single tapered wing according to NACA TN-1270 [15].

The experimental data is matched very well for both numerical models in the linear range of angle of attack (-5° up to approximately 7°). In the nonlinear range the VLM method over-predicts the lift coefficient due to the inherent linear aerodynamic model. The implemented lifting-line method produces good results for lift and drag coefficient in the nonlinear range up to the maximum angle of attack of 21°. This can be achieved in spite of using the linear solver method, because the linearity of the method only influences the calculation of the induced angle of attack, but the calculation of the panel forces and moment is done using the nonlinear airfoil data. This means that at high angles of attack the magnitude of induced velocity will be overestimated from the linear solver method, because it assumes a linear airfoil characteristic. This explains why the lift coefficient is slightly under-estimated in the stall area.

The drag characteristic is also reflected very well by the lifting-line method. The drag calculation at high angles of attack is however strongly influenced by the used airfoil data. This is expected to be the reason for the under-prediction of the drag at high angles of attack, because the used airfoil data only provides data for the profile drag coefficient up to angles of attack of about 12° and was clipped at the boundaries for calculation.

The pitching moment, calculated with the lifting-line method using the quarter chord point as reference point (solid lines in FIG 4), matches the experimental values for zero lift. With nonzero lift the results are diverging from the experiment. As the lift coefficient is matching very well, it is suspected that the reference point of the experimental data was not exactly the quarter chord. A correction of the reference point of 1.5 cm (= 1% MAC) leads to the dashed results in FIG 4, which match the experimental results very well.

4.4.2. Validation of Propeller-Wing Interaction

To validate the implemented interaction between wing and propeller aerodynamics a wing-propeller configuration according to the NACA TN-3307 report [18] has been calculated. The main geometric and aerodynamic properties are listed in TABLE 2.

Property	Value
Wing span	2.08 m
Wing aspect ratio	4.55
Wing taper ratio	0.714
Wing airfoil	NACA0015
Propeller diameter	0.61 m
Velocity in propeller slipstream	25 m/s
Mean Reynolds number	0.8 x 10^6

TABLE 2. Geometric and aerodynamic properties of validation test case according to NACA TN-3307 [18].

The experiments in the wind tunnel were conducted using a semi-span model mounted from the ceiling of the wind tunnel. The experimental setup used two overlapping propellers, but only the results of the tests with the inboard propeller operating were used for this validation of the basic propeller-wing interaction. The tests were conducted for different propeller power settings (including power off condition), velocities, angle of attacks and flap deflections with the dynamic pressure in the slipstream held constant at 383 N/m² at zero angle of attack. The shaft thrust of the propeller was held constant throughout the angle of attack range.

To calculate the non-dimensional lift, drag and moment coefficient as well as the thrust coefficient C_T' according to the NACA report, the dynamic pressure in the slipstream is used:

$$(13)\quad C'_L = \frac{L}{\bar{q}' \cdot S_{Ref}}, C'_D = \frac{D}{\bar{q}' \cdot S_{Ref}}, C'_m = \frac{M}{\bar{q}' \cdot S_{Ref} \cdot c_{Ref}}$$

$$(14)\quad C'_T = \frac{T}{\bar{q}' \cdot A_{Prop}}$$

where S_{Ref} is the reference area and c_{Ref} is the reference chord length. The dynamic pressure in the slipstream is

$$(15)\quad \bar{q}' = \frac{\rho}{2} \cdot V^2 + \frac{T}{A}$$

This is done in order to avoid singularities due to the free stream dynamic pressure going to zero. The different tests with the corresponding thrust, free stream velocity and propeller blade angles $\theta_{0.75}$ (at 75% blade radius) for different thrust coefficients are shown in TABLE 3.

C_T' [-]	V [m/s]	$\bar{q}'$ [N/m²]	T [N]	$\theta_{0.75}$ [°]
0	25.0	383.0	0.0	Off
0.2	22.3	383.0	22.4	20.0
0.5	17.6	383.0	55.6	8.0
0.71	13.5	383.0	78.3	8.0
0.91	24.6	383.0	100.5	8.0
1.0	7.5	383.0	111.2	8.0

TABLE 3. Test conditions of wing-propeller combination according to NACA TN-3307 [18]

The result for the calculation using the linear solver for the test case with no flap deflection is shown in FIG 5. The used airfoil data was based on diagrams from NACA TN-586 [19] for a NACA0015 airfoil.

The lifting-line method used a surface following wake with the trailing vortices leaving the wing at the local flow direction, to account for the different flow conditions at the wing inside and outside the propeller slipstream at high angles of attack. The propeller aerodynamic calculation was done using blade-element momentum theory with Goldstein based modeling of the tangential velocity to achieve a realistic slipstream velocity distribution for the wing section in the slipstream. The propeller-wing iteration was performed by calculating the wing aerodynamics using the slipstream velocity of the propellers and a final propeller calculation using the wing induced velocity at the propeller blades. This setting showed to yield good results if the influence of the wing on the propeller is not too high.

The wing model has been generated using three partitions in order to separately mesh the wing area in the slipstream. 3 panels for the inner section, 10 panels for the middle slipstream section and 5 panels for the outer wing section have been used with a spanwise cosine discretization. The propeller was meshed with 15 panels in radial direction and 4 azimuthal stations. The propeller rotational speed was iterated for the thrust to fit the experimental value given in TABLE 3.

The calculated data shows very good accuracy compared to the experimental results for the calculated angles of attack up to 30°. The lift is predicted very well even

beyond stall. The numerical method underestimates the drag coefficient at high angles of attack and low thrust coefficients. The method is expected to yield better drag results for high angles of attack when using better airfoil data. Also the numerical model overestimates the pitching moment at high angles of attack and high thrust coefficients.

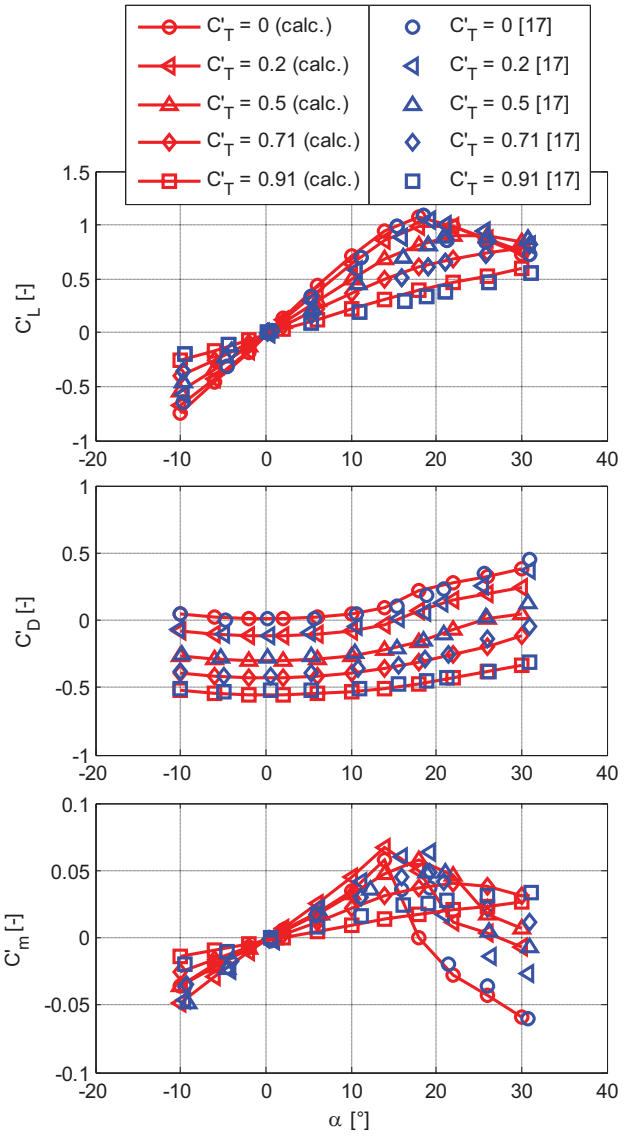

FIG 5. Calculated and experimental results for wing-propeller configuration according to NACA TN-3307 [18] at 0° flap deflection.

5. APPLICATION: "EXTREME STAR" UAV

The aerodynamic framework described in the previous chapter has been applied to the generation of an aerodynamic dataset for a UAV with a large number of flight control inputs.

The aircraft model is shown in FIG 6. The main parameters of the configuration are listed in TABLE 4. The model was built by the Akamodell München on behalf of the Lehrstuhl für Flugsystemdynamik for the purpose of investigating flight dynamics and flight control methods (e.g. control allocation, nonlinear adaptive control) on a UAV with a large number of flight control devices. Therefore the model features aileron and flap control devices on the wing, a canard with variable incidence, a horizontal tail with variable incidence, a rudder on the vertical tail, two wing-mounted propellers with variable vertical tilt angle and one tail-mounted propeller with variable tilt and azimuth angle (see TABLE 5). Additionally an independent control of left side and right side control devices is possible (where applicable).

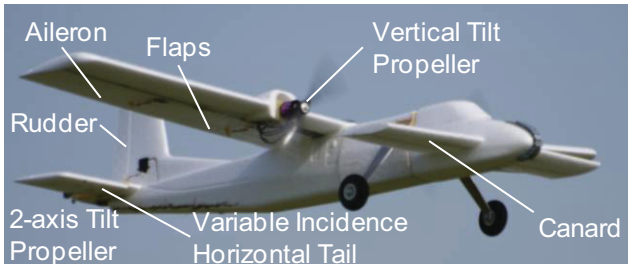

FIG 6. "Extreme Star" UAV during maiden flight and illustration of multiple control devices.

Parameter	Value
Wing span	1.40 m
Canard span	0.58 m
Horizontal tail span	0.42 m
Fuselage length	1.35 m
Left/right motor	2 x max. 500 W (15 s)
Left/right propeller	CAMcarbon 11" x 6"
Tail motor	max. 75 W (15 s)
Tail propeller	GWS 8" x 4.3"

TABLE 4. "Extreme Star" configuration data.

Input	Description	Range
$\eta_{C,l/r}$	Left/right canard deflection	-25°:5°:25°
$\xi_{l/r}$	Left/right aileron deflection	-20°:5°:20°
$\delta_{F,l/r}$	Left/right flap deflection	-20°:5°:25°
$\eta_{E,l/r}$	Left/right elevator deflection	-20°:5°:20°
ζ	Rudder deflection	-30°:5°:30°
$\sigma_{l/r}$	Left/right propeller tilt angle	-25°:6.25°:25°
$n_{l/r}$	Left/right propeller speed	0:4500:13500 rpm
σ_t	Tail propeller tilt angle	-25°…25°
κ_t	Tail propeller azimuth angle	-25°…25°
n_t	Tail propeller speed	0…11000 rpm

TABLE 5."Extreme Star" control inputs.

In order to develop and investigate flight control methods for the UAV, a nonlinear dynamic simulation model of the aircraft has been created. Therefore the aerodynamic forces and moments of the aircraft need to be calculated and stored in aerodynamic data tables. The main requirements for this data table generation are:

- For the data to be suitable for a nonlinear dynamic simulation model, a sufficient range of angles of attack shall be covered including nonlinear effects at high angles of attack.
- The influence of the propellers on the aerodynamics shall be modeled in a suitable way.
- The influence of all control devices shall be modeled (asymmetrically, where applicable) with their nonlinear characteristics (w.r.t the control deflection).
- The computational time for the dataset generation has to be within a feasible limit.

With the aerodynamic framework presented in chapter 3 it is possible to account for the first three aspects. The computational model used for the aerodynamic calculation is shown in FIG 7. The approach of reducing the computational time necessary for creating the aerodynamic dataset will be presented in the following section.

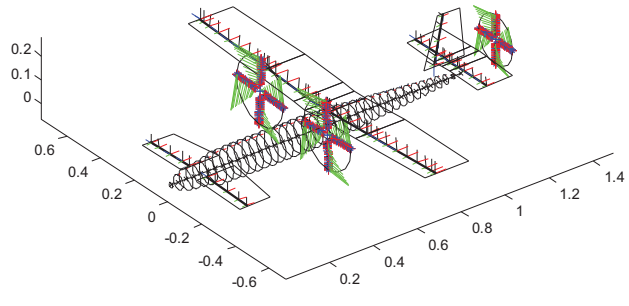

FIG 7. "Extreme Star" calculation geometry with panel data (panel coordinate system and local flow velocity).

5.1. Reducing Computational Time for Aerodynamic Dataset Generation

The aerodynamic dataset to be generated consists of three force coefficients C_D, C_Q, C_L and three moment coefficients C_l, C_m, C_n. The numerical model of the aerodynamics (as described in chapter 4) is able to calculate these coefficients as a function of the six state variables (α, β, V, p, q, r) and the 16 control variables listed in TABLE 5, e.g. the lift coefficient is

$$(16)\quad C_L = f\left(\alpha,\beta,V,p,q,r,\eta_{C,l/r},\xi_{l/r},\delta_{F,l/r},\eta_{E,l/r},\zeta,...\right)$$

Since the computational time for one aerodynamic calculation is approximately two seconds, a real time calculation of the aerodynamics (e.g. at 50 Hz) is not possible. Because of this a pre-calculation of the aerodynamics is necessary. A full-factorial design of the look-up tables has been chosen as the simulation software Matlab Simulink offers a straight forward integration of this type of data table. In a full-factorial design each problem input dimension is discretized on a selected range into a number of breakpoints and the output is calculated for every combination of input values. System response is obtained by linear interpolation of accordingly pre-calculated data. Other types of data fitting capable of handling non-rectangular (scattered) data, such as interpolation using triangularization or linear/nonlinear regression models (e.g. radial basis functions or neural networks), shall not be discussed here.

A full-factorial experimental design for the complete aerodynamic model with 22 input dimensions is not possible within a feasible computational time and would lead to a data amount that cannot be handled in a reasonable way. Therefore a simplification of the data structure has to be found that optimally preserves the characteristics of the original numerical model. The following methods have been used to simplify the dataset:

- Use of aircraft symmetry:
  The aircraft aerodynamics is calculated for the total aircraft, but only the forces and moments of one half are used for dataset generation. The total values are then composed from this half-side datasets (see eq. (21), Index r) added to the results from fuselage and vertical tail. This allows a free asymmetric modeling of the control inputs assuming independence of left and right hand controls, which will be shown later.
- Identification of input dependencies that are not modeled in the numerical calculation [20]:

$$(17)\quad \left.\frac{\partial y}{\partial z_i}\right|_{\vec{z}} = 0, \forall \vec{z} \in D$$

  i.e the input variable z_i does not influence the output y across the entire input variable space. As a consequence of the applied propeller method, only the propeller influence on geometry behind the propeller disk is modeled. Because of this, the tail propeller is completely decoupled from the aircraft aerodynamics and can be neglected in the aerodynamic calculation.
- Identification and/or selection of input variables with linear and additive effect [20]:

$$(18)\quad \left.\frac{\partial y}{\partial z_i}\right|_{\vec{z}} = \text{constant} \neq 0, \forall \vec{z} \in D$$

  For the actual application, the rotational rates p, q, r have been selected as variables with linear effect. For these variables only the linear derivative at each dataset point has to be calculated (see eq. (21)).
- Identification of limited parameter interdependencies [20]:

$$(19)\quad \left.\frac{\partial y}{\partial z_i}\right|_{\vec{z}} = g\left(z_j\right) \neq \text{constant}, \forall \vec{z} \in D,$$

  i.e. the influence of a input variable z_i on the output is nonlinear but only dependent of a subset of input variables z_j. In this case the subspace of the input variables z_j can be used to create a (full-factorial) data table representing the influence of the input variable z_i on the output y.

Practically it is not possible to investigate the gradient information across the entire input variable space. Also the stated conditions might not be exactly true, but rather they are taken as a quantification criterion for the selection of variables to be treated in a special way.

FIG 8 shows the result of an interdependence analysis done at the design point (V = 20 m/s, α = 0°, $n_{l/r}$ = 8000 rpm). It has been used to identify the variables z_j (column), that influence the impact of variable z_i (row) on the aerodynamic coefficients. These variables are then used to create the data table representing the effect of an input z_i. For example the effect of a flap deflection δ_F is identified to be dependent on the angle of attack as well as the propeller speed n and airspeed V (resulting in a certain induced propeller slipstream velocity). In the same manner the independence of left and right hand controls has been shown (not depicted in FIG 8). The interdependence values I_{ij} have been created by comparing the gradient of the aerodynamic coefficients w.r.t. the input parameter z_i for two different values of parameter z_j (the maximum and the design value) using a forward finite difference to approximate the gradient:

$$(20)\quad I_{ij} = \frac{y\left(z_i = z_{i,\max}, z_j = z_{j,\max}\right) - y\left(z_i = z_{i,0}, z_j = z_{j,\max}\right)}{\bar{z}_{i,\max} - \bar{z}_{i,0}} - \frac{y\left(z_i = z_{i,\max}, z_j = z_{j,0}\right) - y\left(z_i = z_{i,0}, z_j = z_{j,0}\right)}{\bar{z}_{i,\max} - \bar{z}_{i,0}}$$

where $\bar{z}$ are the dimensionless input parameters.

C_D C_l C_Q C_m C_L C_n	z_j	V	α	β	η_C	ξ	δ_F	η_E	ζ	σ	n
z_i	V	0 0 0 0 0 0 0 0 0	0,1 0 0 0 0,7 0 0,3 0 0	0 0 0 0 0 0 0 0 0	0 0 0 0 0 0 0 0 0	0 0 0 0 0 0 0 0 0	0 0 0 0 0,1 0 0,1 0 0	0 0 0 0 0,5 0 0,1 0 0	0 0 0 0 0 0 0 0 0	0 0 0 0 0,1 0 0,1 0 0	0 0 0 0 0,1 0 0 0 0
	α	0,1 0 0 0 0,5 0 0,2 0 0	0 0 0 0 0 0 0 0 0	0 0 0 0 0,1 0 0,1 0 0	0 0,1 0 0 0,8 0 0,2 0 0	0 0,3 0 0 0,5 0 0,6 0 0	0 0,1 0 0 0,4 0 0,5 0 0	0 0 0 0 1,1 0 0,3 0 0	0 0 0 0 0 0 0 0 0	0 0,1 0 0 0 0 0,2 0 0	0,1 0,1 0 0 0,6 0 0,4 0 0
	β	0 0 0 0 0 0 0 0 0	0 0 0 0 0,1 0 0,1 0 0	0 0 0 0 0 0 0 0 0	0 0 0 0 0 0 0 0 0	0 0 0 0 0 0 0 0 0	0 0 0 0 0 0 0 0 0	0 0 0 0 0 0 0 0 0	0 0 0 0 0 0 0 0 0	0 0 0 0 0 0 0 0 0	0 0 0 0 0 0 0 0 0
	η_C	0 0 0 0 0 0 0 0 0	0 0,1 0 0 0,8 0 0,2 0 0	0 0 0 0 0 0 0 0 0	0 0 0 0 0 0 0 0 0	0 0 0 0 0 0 0 0 0	0 0 0 0 0 0 0 0 0	0 0 0 0 0 0 0 0 0	0 0 0 0 0 0 0 0 0	0 0 0 0 0 0 0 0 0	0 0 0 0 0 0 0 0 0
	ξ	0 0 0 0 0 0 0 0 0	0 0,3 0 0 0,5 0 0,6 0 0	0 0 0 0 0 0 0 0 0	0 0 0 0 0 0 0 0 0	0 0 0 0 0 0 0 0 0	0 0 0 0 0 0 0 0 0	0 0 0 0 0 0 0 0 0	0 0 0 0 0 0 0 0 0	0 0 0 0 0 0 0 0 0	0 0 0 0 0 0 0 0 0
	δ_F	0 0 0 0 0,1 0 0,1 0 0	0 0,1 0 0 0,4 0 0,5 0 0	0 0 0 0 0 0 0 0 0	0 0 0 0 0 0 0 0 0	0 0 0 0 0 0 0 0 0	0 0 0 0 0 0 0 0 0	0 0 0 0 0 0 0 0 0	0 0 0 0 0 0 0 0 0	0 0 0 0 0 0 0 0 0	0 0,1 0 0 0,2 0 0,2 0 0
	η_E	0 0 0 0 0,4 0 0,1 0 0	0 0 0 0 1,1 0 0,3 0 0	0 0 0 0 0 0 0 0 0	0 0 0 0 0 0 0 0 0	0 0 0 0 0 0 0 0 0	0 0 0 0 0 0 0 0 0	0 0 0 0 0 0 0 0 0	0 0 0 0 0 0 0 0 0	0 0 0 0 0,3 0 0,1 0 0	0 0 0 0 0,7 0 0,2 0 0
	ζ	0 0 0 0 0 0 0 0 0	0 0 0 0 0 0 0 0 0	0 0 0 0 0 0 0 0 0	0 0 0 0 0 0 0 0 0	0 0 0 0 0 0 0 0 0	0 0 0 0 0 0 0 0 0	0 0 0 0 0 0 0 0 0	0 0 0 0 0 0 0 0 0	0 0 0 0 0 0 0 0 0	0 0 0 0 0 0 0 0 0

FIG 8. Matrix showing magnitude of input variable interdependencies: How strong is the influence of variable z_i (row) affected by the variable z_j (column).

State	Description	Range
α	Angle of attack	-27.5°:2.75°:27.5°
β	Angle of sideslip	-15°:5°:15°
V	Airspeed	5, 10, 20 m/s

TABLE 6. Flight state breakpoints for dataset generation.

With these simplifications the system is decomposed into a number of full-factorial datasets. The lift coefficient as an example for a longitudinal coefficient is

$$\begin{aligned} & C_L\left(V,\alpha,\beta,p,q,r,\eta_{C,r/l},\xi_{r/l},\delta_{F,r/l},\eta_{E,r/l},\zeta,\sigma_{r/l},n_{r/l}\right)\cong \\ & C_{L,Fus+VT}\left(\alpha,\beta,\zeta\right) \\ & +C_{L,r}\left(V,\alpha,\beta,\sigma_r,n_r\right)+C_{L,r}\left(V,\alpha,-\beta,\sigma_l,-n_l\right) \\ & +\Delta_{\eta_C}C_{L,r}\left(\alpha,\eta_{C,r}\right)+\Delta_{\eta_C}C_{L,r}\left(\alpha,\eta_{C,l}\right) \\ & +\Delta_{\xi}C_{L,r}\left(\alpha,\xi_r\right)+\Delta_{\xi}C_{L,r}\left(\alpha,\xi_l\right) \\ & +\Delta_{\delta_F}C_{L,r}\left(V,\alpha,n_r,\delta_{F,r}\right)+\Delta_{\delta_F}C_{L,r}\left(V,\alpha,-n_l,\delta_{F,l}\right) \\ & +\Delta_{\eta_E}C_{L,r}\left(V,\alpha,\sigma_r,n_r,\eta_{E,r}\right)+\Delta_{\eta_E}C_{L,r}\left(V,\alpha,\sigma_l,-n_l,\eta_{E,l}\right) \\ & +C_{Lp}\left(\alpha,\beta\right)\cdot p^*+C_{Lq}\left(\alpha,\beta\right)\cdot q^*+C_{Lr}\left(\alpha,\beta\right)\cdot r^* \end{aligned} \tag{21}$$

The rolling moment coefficient as an example for a lateral coefficient is

$$\begin{aligned} & C_l\left(V,\alpha,\beta,p,q,r,\eta_{C,r/l},\xi_{r/l},\delta_{F,r/l},\eta_{E,r/l},\zeta,\sigma_{r/l},n_{r/l}\right)\cong \\ & C_{l,Fus+VT}\left(\alpha,\beta,\zeta\right) \\ & +C_{l,r}\left(V,\alpha,\beta,\sigma_r,n_r\right)-C_{l,r}\left(V,\alpha,-\beta,\sigma_l,-n_l\right) \\ & +\Delta_{\eta_C}C_{l,r}\left(\alpha,\eta_{C,r}\right)-\Delta_{\eta_C}C_{l,r}\left(\alpha,\eta_{C,l}\right) \\ & +\Delta_{\xi}C_{l,r}\left(\alpha,\xi_r\right)-\Delta_{\xi}C_{l,r}\left(\alpha,\xi_l\right) \\ & +\Delta_{\delta_F}C_{l,r}\left(V,\alpha,n_r,\delta_{F,r}\right)-\Delta_{\delta_F}C_{l,r}\left(V,\alpha,-n_l,\delta_{F,l}\right) \\ & +\Delta_{\eta_E}C_{l,r}\left(V,\alpha,\sigma_r,n_r,\eta_{E,r}\right)-\Delta_{\eta_E}C_{l,r}\left(V,\alpha,\sigma_l,-n_l,\eta_{E,l}\right) \\ & +C_{lp}\left(\alpha,\beta\right)\cdot p^*+C_{lq}\left(\alpha,\beta\right)\cdot q^*+C_{lr}\left(\alpha,\beta\right)\cdot r^* \end{aligned} \tag{22}$$

Using this decomposition the complete aerodynamic dataset using the control breakpoints listed in TABLE 5 and the flight state breakpoints listed in TABLE 6 can be calculated in approximately 40 hours on a standard desktop PC.

5.2. Results

The results of the aerodynamic calculation of the "Extreme Star" model are presented in this section. The calculation has been performed using the methods described in chapter 4. The results of the original numerical model of the UAV without any simplifications (*orig.*) are compared to the results obtained by applying the dataset decomposition described in section 5.1 (*comp.*). This is done in order to verify the assumed parameter interdependencies for dataset simplification.

FIG 9 shows the longitudinal coefficients of the model for different symmetric front propeller speeds at V = 20 m/s and zero control deflections. The higher maximum lift at high propeller speeds is mainly due to the higher Reynolds numbers in the slipstream yielding higher maximum airfoil lift. The agreement of the composed data is of course very good because of the zero control inputs. Only at the limits of the angle of attack the composed results are clipped to the α-range boundary value.

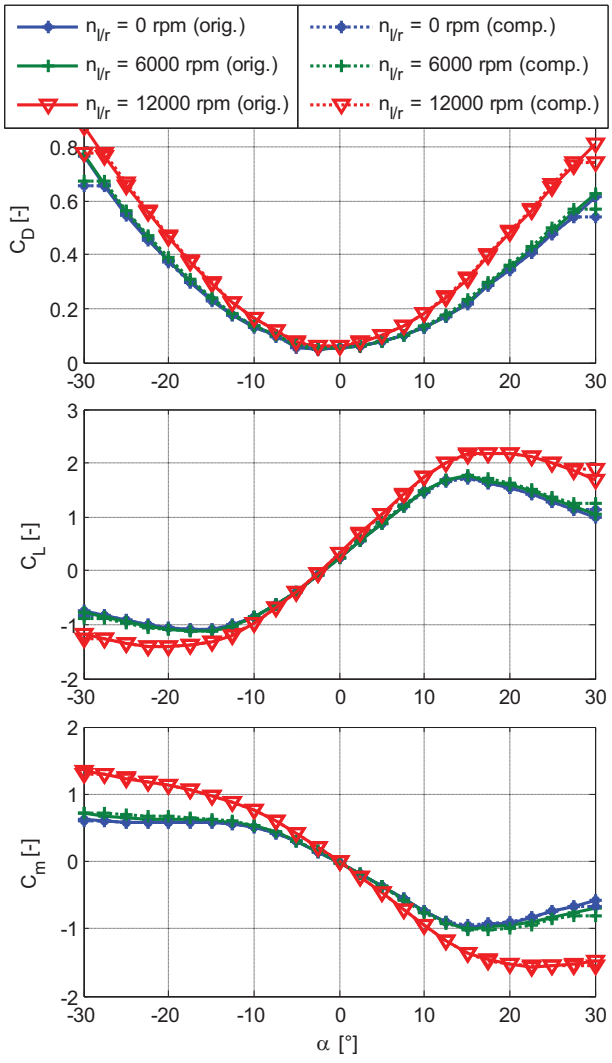

FIG 9. Calculated longitudinal coefficients for different propeller speeds at V = 20 m/s and zero control deflections. Comparison of original and composed model.

FIG 10 and FIG 11 show the calculated pitching moment coefficient for symmetric deflections of the elevator and the canard respectively. The error for the composed dataset model at negative elevator deflections and high angles of attack results from the neglected mutual influence of left and right elevator surface. In the simplified calculation using aircraft symmetry, the left hand side elevator deflection is assumed to be zero, whereas in the depicted case both elevator surfaces have the same deflection.

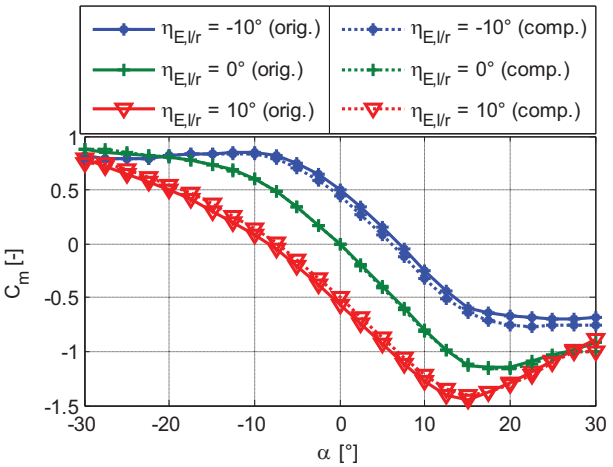

FIG 10. Calculated pitching moment coefficient for different symmetric deflections of elevator at V = 20 m/s and $n_{l/r}$ = 8000 rpm. Comparison of original and composed model.

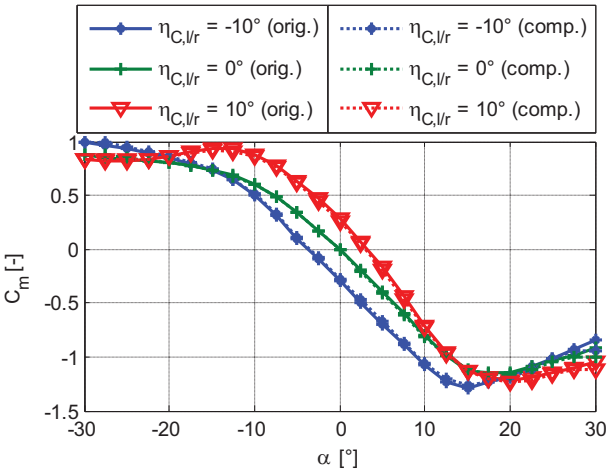

FIG 11. Calculated pitching moment coefficient for different symmetric deflections of canard at V = 20 m/s and $n_{l/r}$ = 8000 rpm. Comparison of original and composed model.

In FIG 12 the lateral coefficients for an anti-symmetric aileron deflection with several other control surfaces deflected are shown. Because of the positive angle of sideslip, the asymmetrically deflected canards and the both clockwise rotating propellers, the lateral coefficients are non-zero even at zero aileron deflection. It can be seen that the effectiveness of the ailerons decreases at high angles of attack with the rolling moment going to zero. Also the good quality of the composed model for this case with strongly coupled control deflections shows that the simplifications introduced for dataset generation are valid.

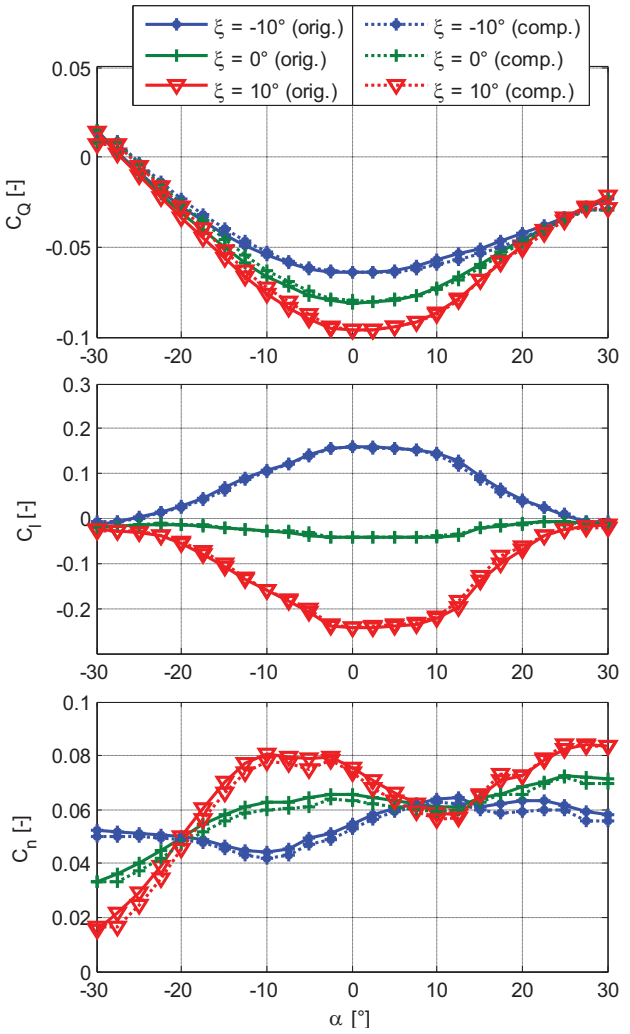

FIG 12. Calculated lateral coefficients for different anti-symmetric deflections of ailerons at V = 20 m/s, β = 5°, $n_{l/r}$ = 9000 rpm and deflected controls ($\eta_{C,l/r}$ = ±5°, $\delta_{F,l/r}$ = 5°, $\eta_{E,l/r}$ = 5°, ζ = -10°, $\sigma_{l/r}$ = 12.5°). Comparison of original and composed model.

The depicted results show the system behavior with the values of the input parameters identical to the chosen breakpoints for dataset generation. The purpose is to show the quality of the original system results and the validity of the introduced decoupled data structure. Subject to current work is the improvement of the dataset design and evaluation. With the currently used linear interpolation the quality of the composed model decreases at intermediate points, especially for parameters with strong nonlinearities, like airspeed or propeller tilt angle. A refinement of the according dimension discretization would lead to better results, but this would also increase the computational time for dataset generation. Therefore other methods like radial basis functions or feed-forward neural networks are currently being investigated to account for nonlinearities in the decoupled sub-datasets.

6. CONCLUSION

The integration of different methods for calculating propeller-wing and body aerodynamics into a geometry framework was presented. The implementation of a

hierarchical geometry parameterization structure allows for easy generation and modification of arbitrary aircraft configurations with complex kinematic properties. Examples for such configurations are aircraft with propeller powered high-lift systems, aircraft with distributed propulsion or Tilt-Wing aircraft. The applied nonlinear lifting-line method for modeling lifting surface aerodynamics and the coupling to blade-element based methods for propeller modeling have been shown to yield good results compared to wind-tunnel experimental data.

The framework was then applied to generate a complete aerodynamic dataset for a nonlinear simulation of a UAV with strong propeller-wing coupling and a large number of control devices. Different methods for reducing the computational time for dataset generation to a reasonable value have been presented and applied, namely the use of aircraft symmetry and the identification of input parameters with linear effect or limited interdependence.

Results of the aerodynamic modeling have been presented, including a comparison of the simplified composed results to the results of the original numerical model without simplifications. It could be shown that the applied simplifications yield good results.

Currently different methods for dataset design and evaluation (radial basis functions and feed-forward neural networks) are being investigated in order to achieve better results compared to the linear interpolation.

7. ACKNOWLEDGEMENTS

The authors would like to thank O. Heinzinger from EADS Innovation Works for supporting the tool development as well as C. Breitsamter and R. Cavallaro for sharing their aerodynamic experience.

8. REFERENCES

[1] R. Fink, "USAF Stability and Control DATCOM," Long Beach, California: McDonnell Douglas Corporation, 1978.

[2] J.L. Hess and W.O. Valarezo, "Calculation of Steady Flow about Propellers using a Surface Panel Method," *Journal of Propulsion and Power*, Vol. 1, 1985, pp. 470-476.

[3] D.P. Witkowski, A.K. Lee, and J.P. Sullivan, "Aerodynamic Interaction between Propellers and Wings," *Journal of Aircraft*, Vol. 26, 1989, pp. 829-836.

[4] P. Lötstedt, "Propeller Slip-Stream Model in Subsonic Linearized Potential Flow," *Journal of Aircraft*, Vol. 29, 1992, pp. 1098-1105.

[5] R.H. Stone, "Aerodynamic Modeling of the Wing–Propeller Interaction for a Tail-Sitter Unmanned Air Vehicle," *Journal of Aircraft*, Vol. 45, 2008, pp. 198-210.

[6] D. Hunsaker and D. Snyder, "A Lifting-Line Approach to Estimating Propeller/Wing Interactions," *Proceedings of the 24th Applied Aerodynamics Conference*, San Francisco, CA, 2006.

[7] W.F. Phillips and D.O. Snyder, "Modern Adaptation of Prandtl's Classic Lifting-Line Theory," *Journal of Aircraft*, Vol. 37, 2000, pp. 662-670.

[8] M.E. Dreier, Introduction to Helicopter and Tiltrotor Flight Simulation, Reston, VA: American Institute of Aeronautics and Astronautics, 2007.

[9] W. Johnson, Helicopter Theory, Mineola, N.Y.: Dover Publications, Inc., 1980.

[10] W.F. Phillips, Mechanics of Flight, Hoboken, New Jersey: John Wiley & Sons Inc, 2004.

[11] D.F. Hunsaker, "A Numerical Blade Element Approach to Estimating Propeller Flowfields," *Proceedings of the AIAA Aerospace Sciences Meeting and Exhibit*, Reno, Nevada, 2007.

[12] B.W. McCormick, Aerodynamics of V/STOL Flight, San Diego, California: Academic Press, Inc., 1967.

[13] H. Schlichting and E. Truckenbrodt, Aerodynamik des Flugzeuges, Zweiter Band, Berlin: Springer-Verlag, 2001.

[14] J. Katz and A. Plotkin, Low-Speed Aerodynamics: From Wing Theory to Panel Methods, Singapore: McGraw-Hill, Inc., 1991.

[15] R.H. Neely, T.V. Bollech, G.C. Westrick, and R.R. Graham, Experimental and Calculated Characteristics of Several NACA 44-Series Wings with Aspect Ratios of 8, 10, and 12 and Taper Ratios of 2.5 and 3.5, Washington: National Advisory Committee for Aeronautics, Technical Note No. 1270, 1947.

[16] T. Melin, A Vortex Lattice MATLAB Implementation for Linear Aerodynamic Wing Applications, Master Thesis, Department of Aeronautics, Royal Institute of Technology (KTH), 2000.

[17] I.H. Abbott and A.E. von Doenhoff, Theory of Wing Sections, New York: Dover Publications, Inc., 1959.

[18] R.E. Kuhn and J.W. Draper, An Investigation of a Wing-Propeller Configuration Employing Large-Chord Plain Flaps and Large-Diameter Propellers for Low-Speed Flight and Vertical Take-Off, Langley Field, Va.: National Advisory Committee for Aeronautics, Technical Note No. 3307, 1943.

[19] E.N. Jacobs and A. Sherman, Airfoil Section Characteristics as Affected by Variations of the Reynolds Number, Langley Field, Va.: National Advisory Committee for Aeronautics, Technical Report No. 586, 1939.

[20] A. Forrester, A. Sobester, and A. Keane, Engineering Design via Surrogate Modelling: A Practical Guide, Chichester, UK: John Wiley & Sons Inc, 2008.